Received: 13 October 2020 | Revised: 26 February 2021 | Accepted: 1 March 2021

DOI: 10.1111/ter.12527

RESEARCH ARTICLE

Terra Nova WILEY

Magma dehydration controls the energy of recent eruptions at Mt. Etna volcano

Francesco Zuccarello[1] | **Federica Schiavi**[2] | **Marco Viccaro**[1,3]

[1]Dipartimento di Scienze Biologiche Geologiche e Ambientali, Università degli Studi di Catania, Catania, Italy

[2]Université Clermont-Auvergne, CNRS, IRD, OPGC, Laboratoire Magmas et Volcans, Clermont-Ferrand, France

[3]Istituto Nazionale di Geofisica e Vulcanologia – Sezione di Catania, Osservatorio Etneo, Catania, Italy

Correspondence
Marco Viccaro, Università degli Studi di Catania, Dipartimento di Scienze Biologiche Geologiche e Ambientali, Corso Italia 57, I-95129 Catania, Italy.
Email: m.viccaro@unict.it

Funding information
Università di Catania

Abstract

Olivine-hosted melt inclusions (MIs) from tephra of the recent 2013–2018 activity at Mt. Etna were investigated for assessing the chemical evolution of magmas and quantifying their pre-eruptive volatile budget. Microanalyses revealed two types of MIs present in all investigated eruptions; the inclusions, particularly the less evolved ones, appear to have experienced water loss coupled with SiO_2 depletion. Restoration of the original SiO_2-H_2O concentrations provides consistency with the thermodynamic modelling of magma evolution. The two types of MIs developed during crystallization of olivine plus clinopyroxene between 200 and 100 MPa, where magmas also experienced CO_2 flushing. Degassing processes at these levels are responsible for water depletion in the melt and diffusive water loss from inclusions. Our data suggest that initial water budget is unchanged all over the last 20 years, reflecting therefore a potential in triggering highly explosive eruptions depending on degassing dynamics under open versus closed system conditions at shallow levels.

Statement of significance

An extensive dataset of major and trace elements, together with H_2O, CO_2, S, Cl and F, has been obtained on melt inclusions entrapped in olivine crystals from three selected recent eruptions occurred at Mt. Etna volcano. These data are novel, original and timely considering that volatile concentrations for post-2011 Mt. Etna magmas are scarce in literature up to date. Assessing of the original volatile budgets of magmas and how their volatile load changes throughout the present configuration of the plumbing system is crucial to reconstruct the degassing dynamics of magmas and to identify the causes leading to energetic versus quiet eruptions of the volcano.

1 | INTRODUCTION

A new eruptive cycle started in January 2011 at Mt. Etna (Southern Italy). The activity was mainly explosive, with 44 episodes of lava fountaining occurred at the New South East Crater (NSEC) during the 2011–2013 period (e.g. Behncke et al., 2014; Giuffrida & Viccaro, 2017), culminating with the most powerful paroxysmal eruptions of the last 20 years at the Voragine crater (VOR) on December 2015 and May 2016 (Cannata et al., 2018). A frequency decrease in eruptive episodes marked the post-2016 activity, shifting to more effusive behaviours (Viccaro et al., 2019). Efforts in constraining spatial and temporal evolution of magma dynamics enlightened the complex plumbing system underneath the volcano (e.g. Cannata et al., 2015, 2018; Viccaro et al., 2016, 2019), although few data on volatile concentrations for the post-2011 magmas are currently available (Gennaro et al., 2019). Furthermore, these data suggest rather degassed magma compositions, which are in contrast with the eruptive behaviour observed at the volcano.

We provide here a new dataset of major and trace element compositions and volatile contents (i.e. H_2O, CO_2, S, Cl, F) in olivine-hosted

melt inclusions (MIs) selected from tephra emitted during variably energetic eruptions at Mt. Etna, namely: the mostly effusive flank eruption of December 24–27, 2018; the mid-intensity paroxysmal eruption occurred at NSEC on February 19, 2013; the highly energetic paroxysm of December 3, 2015 occurred at VOR. Assessing the original magma volatile budgets and how their load changes over space and time is crucial to reconstruct the degassing dynamics and to identify causes leading to energetic versus quiet eruptions.

2 | COMPOSITIONS OF THE OLIVINE-HOSTED MIs

Olivine crystals were hand-picked from tephra smaller than 1.5 cm and prepared for in situ microanalyses on MIs including measurements of major elements, S, Cl and F by EMPA, trace element abundances by LA-ICP-MS and determination of H_2O and CO_2 concentrations by FTIR and Raman spectroscopy (see Supporting Information 1). MIs from the three eruptive episodes have similar major element compositions after correction for post-entrapment crystallization [PEC calculated through Petrolog3 software (Danyushevsky & Plechov, 2011) is <13%; Tables S1 and S2 in Supporting Information 2]. Considering SiO_2, CaO and alkali elements, our data suggest the existence of two types of MIs (Figure 1). The type 1 MIs are entrapped in $Fo_{79\text{-}85}$ olivines; they are more basic (SiO_2 42.7–45.7 wt%; Mg# 55–60), with $Na_2O + K_2O$ in the range 5.1–6.2 wt% and CaO 9.9–12.5 wt%. The type 2 MIs are found in $Fo_{69\text{-}79}$ olivines; they are more evolved (SiO_2 46.5–51.2 wt%; Mg# 40–54), with $Na_2O + K_2O$ in the range 6.2–8.3 wt% and CaO 6.1–9.7 wt%. Some type 1 inclusions have anomalously low SiO_2 (~42.7 wt%), which is an odd feature for volcanic rocks erupted at Mt. Etna.

Low H_2O (0.4–2.4 wt%; Figure 2) and CO_2 (46–849 ppm; Figure 3) contents make both types of MIs peculiar if compared to products erupted in the 2001 and 2002–2003 eruptions (Métrich et al., 2004; Spilliaert et al., 2006). Maximum H_2O concentrations were found in type 1 MIs, which display higher average H_2O contents than type 2 MIs. Nonetheless, some type 1 MIs entrapped in high-Fo olivine (>Fo_{80}), especially from the December 2018 eruption, occasionally show very low H_2O contents (~0.47 wt%), sometimes correlated with the lowest SiO_2 contents observed in type 1 MIs. Type 1 MIs are generally characterized by higher CO_2 concentrations than type 2 MIs for all selected eruptive episodes; slight CO_2 enrichment at low H_2O content has also been observed for some type 1 MIs (Figure 3). Sulphur (172–3,072 ppm), Cl (870–2,884 ppm) and F (670–1,546 ppm) concentrations are comparable for MIs of the three eruptive episodes

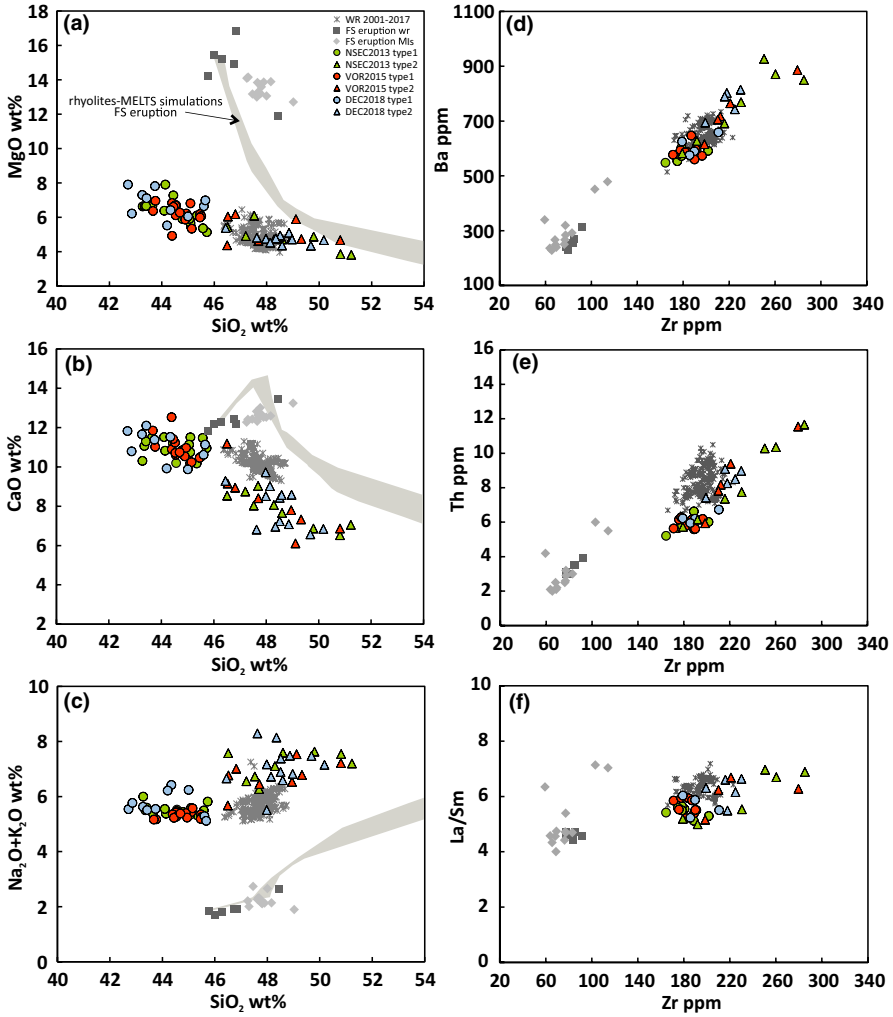

FIGURE 1 Selected major, trace elements and La/Sm plotted against SiO_2 (wt%) and Zr (ppm) respectively. Circles indicate type 1 melt inclusions (MIs), whereas type 2 are represented by triangles; selected eruptions are distinguished by colour: green for the February 19, 2013, eruption at NSEC (NSEC 2013); red for the paroxysm of December 3, 2015 at VOR (VOR 2015); light blue for the flank eruption occurred on December 24–27, 2018 (DEC 2018). Type 1 MIs show very low SiO_2 contents compared to the whole-rock compositions from the 2011–2017 period (grey asterisks) and to the most primitive whole-rock (grey squares) and MI (grey diamonds) compositions erupted during the 3,930 BP eruption (Kamenetsky et al., 2007). The dark grey area represents the rhyolite-MELTS simulation starting from the composition of the most primitive melt from the 3,930 BP eruption at P = 500 MPa, T = 1,300°C, H_2O = 3.8 wt%, and CO_2 = 3,280 ppm and variable fO_2 buffers [i.e. Quartz-Fayalite-Magnetite (QFM) and Nickel Nickel Oxide (NNO)] [Colour figure can be viewed at wileyonlinelibrary.com]

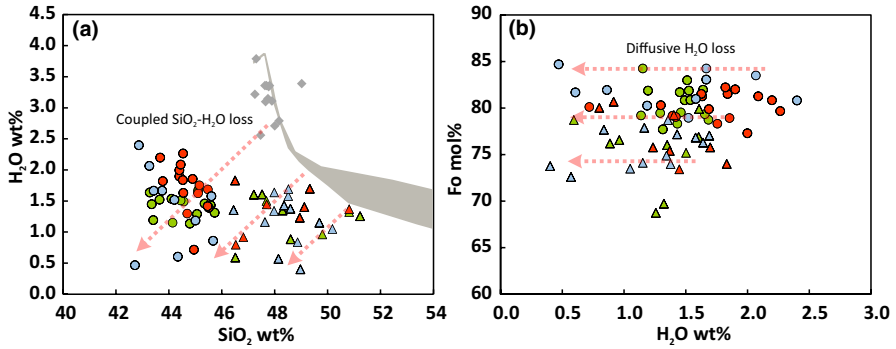

FIGURE 2 Water contents measured in melt inclusions (MIs) plotted against (a) SiO_2 wt% in the MI glass and (b) Fo mol.% of the hosting olivine. The grey area in (a) represents rhyolite-MELTS simulations starting from the primitive melts erupted during the 3,930 BP eruption. The simulation predicts higher H_2O contents than those measured in the studied MIs. The dashed red arrows indicate the hypothetical trend caused by diffusive H_2O loss, which is coupled to SiO_2 depletion [Colour figure can be viewed at wileyonlinelibrary.com]

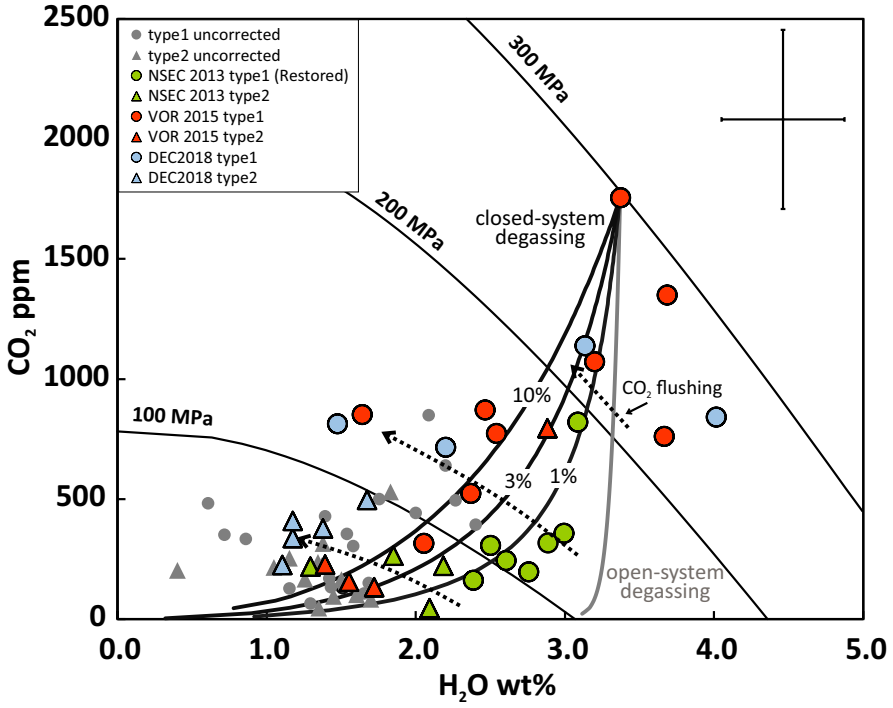

FIGURE 3 Diagram showing unrestored and restored H_2O-CO_2 melt inclusions (MIs) compositions (see colour legend) with associated degassing paths calculated using VOLATILECALC (Newman & Lowenstern, 2002). Open-system degassing (grey curve) from 300 MPa, H_2O = 3.37 wt%, CO_2 = 1,754 ppm cannot predict restored MIs, whereas at same conditions closed-system degassing curves (black lines) defined with initial gas phase ranging from 1% to 10% well reproduce the observed data. Dashed black arrows highlight the occurrence of CO_2 flushing at pressure lower than 200 MPa. The error bars indicate the largest uncertainties estimated for the highest H_2O and CO_2 concentrations, taking into account the error propagation in the restoration of original compositions [Colour figure can be viewed at wileyonlinelibrary.com]

(Figure S1 in Supporting Information 2). Sulphur shows progressive decrease from type 1 to type 2 MIs, whereas F concentrations are higher in type 2 than type 1 MIs; Cl contents are comparable in the two groups, but a few type 2 MIs show the highest values.

Type 1 MIs from all products show similar concentrations of LILEs, HFSEs and REEs. Type 2 MIs generally display trace element concentrations higher than type 1 MIs (Figure 1; Table S3 in Supporting Information 2), also covering wider compositional ranges. Ratios of variably incompatible trace elements (i.e. La/Sm, Ba/Sr, Zr/Nb; Figure 1; Figure S1 in Supporting Information 2) support analogous geochemical signature for MIs coming from the three eruptions, with minor differences between the two types of MIs.

3 | DISCUSSION

Thermodynamic simulations performed by rhyolite-MELTS (Ghiorso & Gualda, 2015; Gualda et al., 2012) fix the evolutionary path for the

post-2011 Mt. Etna magmas. The most primitive known compositions at Mt. Etna were found in MIs entrapped in Fo_{90-91} olivines erupted during the FS eruption (3,930 BP; Kamenetsky et al., 2007), so they could be reasonably assumed as starting melt composition for the thermodynamic simulation. However, no solution at different conditions (i.e. fO_2 and d*P*/d*T*) provides compositions of the studied MIs. In fact, the FS products have SiO_2 concentrations (~47.3–49.0 wt%) higher than those measured in the most basic type 1 MIs, with no possibilities to reproduce differentiation paths fitting such low SiO_2 concentrations (Figures 1 and 2a). Furthermore, historical products show different geochemical signature if compared to volcanic rocks emitted particularly after the 1971 benchmark (e.g. Viccaro & Zuccarello, 2017). This points out that FS melts are not the parental magmas for recent products.

H_2O contents measured in MIs of the post-2011 activity are much lower than concentrations predicted from thermodynamic models, a feature particularly evident for some basic type 1 MIs entrapped in high-Fo olivine (80–85 mol.%), indicating entrapment pressures < 130 MPa (calculated through VOLATILECALC; Newman & Lowenstern, 2002) during crystallization of such olivine populations. A large variability in water content (ΔH_2O~2 wt%) characterizes MIs entrapped in olivine with similar Fo contents (Figure 2b), highlighting that water loss may be responsible for H_2O depletion in MIs. Water loss in MIs has been commonly observed in both natural and experimental samples (e.g., Barth et al., 2019; Gaetani et al., 2012; Lloyd et al., 2013; Portnyagin et al., 2008, 2019). Magma degassing during ascent and storage at shallower levels of the plumbing system may induce re-equilibration of MIs, which release H_2O to the external melt by diffusion through the olivine lattice. Two main mechanisms of H^+ transport have been recognized: (1) the fastest proton–polaron exchange, where redox reactions occur between H^+ and polaron on Fe^{3+} atoms occupying the octahedral sites (Gaetani et al., 2012; Kohlstedt & Mackwell, 1998; Mackwell & Kohlstedt, 1990); (2) incorporation of H^+ in olivine through metal-vacancy defects (Demouchy & Mackwell, 2003, 2006; Kohlstedt & Mackwell, 1998). A recent experimental study on Ti-depleted calc-alkaline products erupted at Klyuchevskoy volcano revealed a coupled behaviour of H_2O and SiO_2 during re-equilibration of MIs with the external matrix (cf. Portnyagin et al., 2019). A concomitant increase of H_2O and SiO_2 in MIs was observed during MIs rehydration, whereas reversal experiment showed the process is reversible.

These findings provide a possible explanation for occurrence of strong SiO_2 depletion in MIs, although no experimental studies have been conducted on olivine crystallized from Etna alkaline melts, which means data useful for disambiguation of possible mechanisms of H^+ incorporation and transport in Etnean olivines are not available. Few FTIR spectra collected on olivine crystals close to inclusions display, however, the presence of a broad band located at 3,160 cm^{-1} and a peak at 3,220 cm^{-1}. These characteristic bands are related to H^+ in point defects associated with metal vacancies (M1 for 3,160 cm^{-1} and M2 for 3,220 cm^{-1}; Berry et al., 2005; Portnyagin et al., 2019), whereas other bands related to Si vacancies, Ti and Fe^{3+} point defects were not recognized (Figure S2 in Supporting Information 2). The correlation between low H_2O and SiO_2 contents, together with the characteristic spectral bands of H^+ in metal vacancies, suggests that loss of SiO_2 and H_2O could be due to metal defect formation in olivine crystallizing on MI walls during dehydration.

Reconstruction of the pristine H_2O and SiO_2 contents before water loss was made for MIs of the post-2011 activity. SiO_2 content of whole rocks was used as a pristine value to recalculate original H_2O-SiO_2 compositions in MIs, assuming that MIs were characterized initially by the same Si-saturation index as their host rocks (Portnyagin et al., 2019). Bulk rock compositions in equilibrium with olivines with variable forsteritic content were selected from the record since 2001 (Figure S3 and Table S4 in Supporting Information 2; Viccaro & Cristofolini, 2008), avoiding samples with distinctive features inherited by accumulation of specific mineral phases (e.g. amphibole; cf. Viccaro et al., 2006). PEC was performed on restored SiO_2-H_2O compositions. Recalculations suggest that, on average, 4.80 and 3.42 wt% of SiO_2 should be added, respectively, to the composition of type 1 and type 2 MIs from the 2013–2015 paroxysms, whereas on average 7.20 wt% (type 1 MIs) and 4.03 wt% (type 2 MIs) of SiO_2 is needed for MIs of the 2018 eruption, thus indicating that MIs from the 2018 eruption were affected more extensively by water loss. Recalculated MI compositions showing the highest addition of SiO_2 also display the highest PEC, supporting the idea that crystallization on MI walls may be also controlled by the extent of water loss. This would lead to formation of metal vacancies, which migrate away from the inclusion rim exchanging Fe and Mg (Portnyagin et al., 2019). In absence of experimental data, we used an intermediate molar proportion ($\Delta H_2O/\Delta SiO_2 = 1$), among those defined by Portnyagin et al. (2019), for restoring H_2O compositions as a function of the SiO_2 percentage added to MIs. Restored maximum concentration of H_2O is 4.02 wt% (Figure 3), consistent with values measured in MIs from products of the 2001 and 2002–2003 eruptions (Métrich et al., 2004; Spilliaert et al., 2006).

Low entrapment pressures are also linked to low CO_2 contents measured in glasses. Recent studies demonstrated that most of CO_2 in MIs can be lost from the melt to the shrinkage bubble (Hartley et al., 2014; Moore et al., 2018; Wallace et al., 2015). In order to evaluate this effect, we restored the bulk CO_2 content of MIs by adopting the approach of Wallace et al. (2015) using: (1) VOLATILECALC (Newman & Lowenstern, 2002) to determine the saturation pressure and CO_2 mol.% in the vapour phase in equilibrium with the entrapped liquid, knowing the H_2O-CO_2 dissolved in the melt; and (2) a modified Redlich-Kwong equation of state (Kerrick & Jacobs, 1981) to calculate the molar volume of the H_2O-CO_2 mixture in the vapour phase.

The highest entrapment pressure for the studied MIs from the post-2011 activity was constrained at 300 MPa based on the restored H_2O and CO_2 concentrations at 3.37 wt% and 1,754 ppm, respectively (Figure 3). Restored MIs compositions from the 2013 eruption can be modelled through a closed-system degassing starting from these conditions with 1% of initial gas phase, whereas most of MI compositions from the 2015–2018 eruptions can be reproduced by increasing this parameter at 10%. Such variability in H_2O-CO_2

contents may reflect the occurrence of CO_2 flushing in the upper plumbing system affecting mostly the portion below 200 MPa (cf. Collins et al., 2009). The effect of flushing leads to deviation from the expected open-system degassing as a function of the CO_2 amount fluxed from deeper levels, producing melt dehydration similar to closed-system conditions.

Improvements of thermodynamic modelling were achieved in two-step modelling, using the restored SiO_2-H_2O-CO_2 compositions of MIs (Figure 4). The most primitive inclusion (DECG22MI20, Mg# = 60.3; Table S5 in Supporting Information 2) was used as starting melt for the first step, constraining the initial conditions as follows: T = 1,140°C, P = 300 MPa, fO_2 at the QFM buffer, 4.02 wt% of H_2O and 1,754 ppm of CO_2; the first step ended at T = 1,110°C and P = 210 MPa. The initial melt composition for the second step was fixed starting from the last melt obtained in the first step, then constraining T = 1,110°C, P = 210 MPa, fO_2 at the QFM buffer and H_2O at 3.20 wt% and CO_2 at 1,072 ppm to take into account the effect of CO_2 flushing at 200 MPa. The final T was fixed at 1,064°C (Calvari et al., 1994) and pressure close to surface conditions. Olivine is the sole phase controlling the melt evolution during the first step, changing from Fo_{82} to Fo_{80}. The transition from type 1 to type 2 MIs occurs during the second step, when augitic clinopyroxene in equilibrium with $Fo_{78\text{-}79}$ olivine coexists on the liquidus at 120 MPa, then followed by magnetite at lower pressure. Consistently, small differences in La/Sm and Zr/Nb between the two types of MIs can be accounted for by fractionation of augitic clinopyroxene. Increasing Ba/Sr, which is only observed within the type 2 MIs, is controlled by the late crystallization of plagioclase. Although restoring of MIs compositions following Portnyagin et al. (2019) strongly improved the consistency of thermodynamic models, experiments on natural Etnean olivines are recommended to investigate the mechanism of H^+ diffusion in olivine and quantify a reliable degree of water loss.

Our model provides important indications about the initial volatile budget of recent Mt. Etna magmas. CO_2 flushing in the upper plumbing system has been invoked in previous studies as the main cause for production of dehydrated melts erupted after the benchmark represented by the 2001 eruption (Collins et al., 2009). However, a careful evaluation of processes affecting the original compositions of MIs highlights how magmas erupted during 2013–2018 activity are characterized by a fairly high pristine volatile load, i.e. comparable to that measured in the gas-rich products emitted during the 2001 and 2002–2003 eruptions. This implies that the deep plumbing system is able to supply volatile-rich magmas potentially triggering intense eruptive phenomena at any time. The open versus closed degassing conditions experienced by magmas at shallow levels (<200 MPa) control the final volatile cargo and the eruption intensity. Although the reconstructed H_2O-CO_2 MI compositions simulate a closed-system degassing due to continuous gas input from depth, storage dynamics and the efficient transfer across the upper plumbing system of Mt. Etna now allow loss of substantial water load from magmas without relevant accumulation. Under these conditions, the final eruptive behaviour, from effusive up to vigorous lava fountaining, could be chiefly related to kinetics of magma ascent.

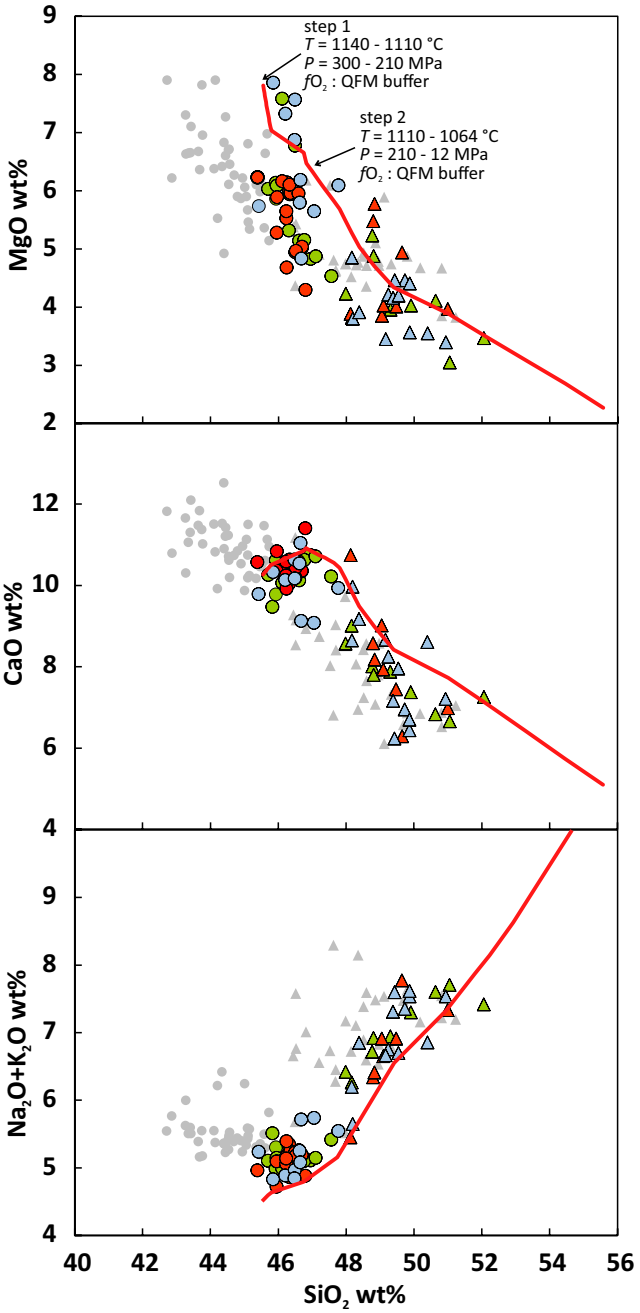

FIGURE 4 Major element compositions in restored melt inclusions (MIs) after correction for SiO_2-H_2O loss. Unrestored MIs are reported for comparison (symbols as in Figure 3). Results from rhyolite-MELTS simulations on restored MIs (red line) and parameters used for each step of simulation are reported [Colour figure can be viewed at wileyonlinelibrary.com]

ACKNOWLEDGEMENTS

Francesco Zuccarello acknowledges the PhD fellowship and two PhD research grants from the University of Catania. This work was supported by the funding program PIACERI 2020-22 of the University of Catania, project PAROSSISMA, code 22722132140 (Principal Investigator M. Viccaro). We are indebted to Jean-Luc Devidal (Laboratoire Magmas et Volcans) for his guidance during EMPA

and LA-ICPMS data acquisition. Thorough reviews provided by the Associate Editor, Helena Albert and an Anonymous Reviewer greatly helped in improving the early submitted version of the manuscript.

CONFLICT OF INTEREST

The authors declare no financial or other conflicts of interests for this work.

DATA AVAILABILITY STATEMENT

The data that support the findings of this study are available in the Supporting Information of this article.

REFERENCES

Barth, A., Newcombe, M. E., Plank, T., Gonnermann, H., Hajimirza, S., Soto, G. J., Saballos, A., & Hauri, E. (2019). Magma decompression rate correlates with explosivity at basaltic volcanoes – Constraints from water diffusion in olivine. *Journal of Volcanology and Geothermal Research*, *387*, 106664. https://doi.org/10.1016/j.jvolgeores.2019.106664

Behncke, B., Branca, S., Corsaro, R. A., De Beni, E., Miraglia, L., & Proietti, C. (2014). The 2011–2012 summit activity of Mount Etna. Birth, growth and products of the new SE crater. *Journal of Volcanology and Geothermal Research*, *270*, 10–21. https://doi.org/10.1016/j.jvolgeores.2013.11.012

Berry, A. J., Hermann, J., O'Neill, H. S. C., & Foran, G. J. (2005). Finger printing the water site in mantle olivine. *Geology*, *33*, 869–872. https://doi.org/10.1130/G21759.1

Calvari, S., Coltelli, M., Neri, M., Pompilio, M., & Scribano, V. (1994). The 1991–1993 Etna eruption: Chronology and lava. *Acta Vulcanologica*, *4*, 1–14.

Cannata, A., Di Grazia, G., Giuffrida, M., Gresta, S., Palano, M., Sciotto, M., Viccaro, M., & Zuccarello, F. (2018). Space-time evolution of magma storage and transfer at Mt.Etna volcano (Italy). The 2015–2016 reawakening of Voragine crater. *Geochemistry, Geophysics, Geosystems*, *19*, 471–495. https://doi.org/10.1002/2017GC007296

Cannata, A., Spedalieri, G., Behncke, B., Cannavò, F., Di Grazia, G., Gambino, S., Gresta, S., Gurrieri, S., Liuzzo, M., & Palano, M. (2015). Pressurization and depressurization phases inside the plumbing system of Mount Etna volcano: Evidence from a multiparametric approach. *Journal of Geophysical Research*, *120*, 5965–5982. https://doi.org/10.1002/2015JB012227

Collins, S. J., Pyle, D. M., & Maclennan, J. (2009). Melt inclusions track pre-eruption storage and dehydration of magmas at Etna. *Geology*, *37*, 571–574. https://doi.org/10.1130/G30040A.1

Danyushevsky, L. V., & Plechov, P. (2011). Petrolog3: Integrated software for modeling crystallization processes. *Geochemistry, Geophysics, Geosystems*, *12*, Q07021. https://doi.org/10.1029/2011GC003516

Demouchy, S., & Mackwell, S. J. (2003). Water diffusion in synthetic iron-free forsterite. *Physics and Chemistry of Minerals*, *30*, 486–494. https://doi.org/10.1007/s00269-003-0342-2

Demouchy, S., & Mackwell, S. J. (2006). Mechanisms of hydrogen incorporation and diffusion in iron-bearing olivine. *Physics and Chemistry of Minerals*, *33*, 347–355. https://doi.org/10.1007/s00269-006-0081-2

Gaetani, G. A., O'Leary, J. A., Shimizu, N., Bucholz, C. E., & Newville, M. (2012). Rapid reequilibration of H_2O and oxygen fugacity in olivine-hosted melt inclusions. *Geology*, *40*, 915–918. https://doi.org/10.1130/G32992.1

Gennaro, E., Iacono-Marziano, G., Paonita, A., Rotolo, S. G., Martel, C., Rizzo, A. L., Pichavant, M., & Liotta, M. (2019). Melt inclusions track melt evolution and degassing of Etnean magmas in the last 15 ka. *Lithos*, *324–325*, 716–732. https://doi.org/10.1016/j.lithos.2018.11.023

Ghiorso, M. S., & Gualda, G. A. R. (2015). An H_2O–CO_2 mixed fluid solubility model compatible with rhyolite-MELTS. *Contributions to Mineralogy and Petrology*, *169*, 53. https://doi.org/10.1007/s00410-015-1141-8

Giuffrida, M., & Viccaro, M. (2017). Three years (2011–2013) of eruptive activity at Mt. Etna. Working modes and timescales of the modern volcano plumbing system from micro-analytical studies of crystals. *Earth-Science Reviews*, *171*, 289–322. https://doi.org/10.1016/j.earscirev.2017.06.003

Gualda, G. A. R., Ghiorso, M. S., Lemons, R., & Carley, T. L. (2012). Rhyolite-MELTS: A modified calibration of MELTS optimized for silica-rich, fluid-bearing magmatic systems. *Journal of Petrology*, *53*, 875–890. https://doi.org/10.1093/petrology/egr080

Hartley, M. E., Maclennan, J., Edmonds, M., & Thordarson, T. (2014). Reconstructing the deep CO_2 degassing behaviour of large basaltic fissure eruptions. *Earth and Planetary Science Letters*, *393*, 120–131. https://doi.org/10.1016/j.epsl.2014.02.031

Kamenetsky, V. S., Pompilio, M., Metrich, N., Sobolev, A. V., Kuzmin, D. V., & Thomas, R. (2007). Arrival of extremely volatile-rich high-Mg magmas changes explosivity of Mount Etna. *Geology*, *35*, 255–258. https://doi.org/10.1130/G23163A.1

Kerrick, D. M., & Jacobs, G. K. (1981). A modified Redlich-Kwong equation for H_2O, CO_2 and H_2O-CO_2 mixtures at elevated pressures and temperatures. *American Journal of Science*, *281*, 735–767. https://doi.org/10.2475/ajs.281.6.735

Kohlstedt, D. L., & Mackwell, S. J. (1998). Diffusion of hydrogen and intrinsic point defects in olivine. *Zeitschrift Für Physikalische Chemie*, *207*, 147–162. https://doi.org/10.1524/zpch.1998.207.Part_1_2.147

Lloyd, A., Plank, T., Ruprecht, P., Hauri, E., & Rose, W. (2013). Volatile loss from melt inclusions in pyroclasts of differing sizes. *Contributions to Mineralogy and Petrology*, *165*, 129–153. https://doi.org/10.1007/s00410-012-0800-2

Mackwell, S. J., & Kohlstedt, D. L. (1990). Diffusion of hydrogen in olivine. Implications for water in the mantle. *Journal of Geophysical Research*, *95*, 5079–5088. https://doi.org/10.1029/JB095iB04p05079

Métrich, N., Allard, P., Spilliaert, N., Andronico, D., & Burton, M. (2004). 2001 flank eruption of the alkali- and volatile-rich primitive basalt responsible for Mount Etna's evolution in the last three decades. *Earth and Planetary Science Letters*, *228*, 1–17. https://doi.org/10.1016/j.epsl.2004.09.036

Moore, R. L., Mirinov, N., Portnyagin, M., Gazel, E., & Bodnar, R. J. (2018). Volatile contents of primitive bubble-bearing melt inclusions from Klyuchevskoy volcano, Kamchatka: Comparison of volatile contents determined by mass-balance versus experimental homogenization. *Journal of Volcanology and Geothermal Research*, *358*, 124–131. https://doi.org/10.1016/j.jvolgeores.2018.03.007

Newman, S., & Lowenstern, J. B. (2002). VolatileCalc: A silicate melt–H_2O–CO_2 solution model written in Visual Basic for excel. *Computers & Geosciences*, *28*, 597–604. https://doi.org/10.1016/S0098-3004(01)00081-4

Portnyagin, M., Almeev, R., Matveev, S., & Holtz, F. (2008). Experimental evidence for rapid water exchange between melt inclusions in olivine and host magma. *Earth and Planetary Science Letters*, *272*, 541–552. https://doi.org/10.1016/j.epsl.2008.05.020

Portnyagin, M., Mirinov, N., Botcharnikov, R., Gurenko, A., Almeev, R. R., Luft, C., & Holtz, F. (2019). Dehydration of melt inclusions in olivine and implications for the origin of silica-undersaturated island-arc melts. *Earth and Planetary Science Letters*, *517*, 95–105. https://doi.org/10.1016/j.epsl.2019.04.021

Spilliaert, N., Allard, P., Métrich, N., & Sobole, A. (2006). Melt inclusion record of the conditions of ascent, degassing and extrusion of volatile-rich alkali basalt during the powerful 2002 flank eruption

of Mount Etna (Italy). *Journal of Geophysical Research*, *111*, B04203, https://doi.org/10.1029/2005JB003934

Viccaro, M., & Cristofolini, R. (2008). Nature of mantle heterogeneity and its role in the short-term geochemical and volcanological evolution of Mt. Etna (Italy). *Lithos*, *105*, 272–288. https://doi.org/10.1016/j.lithos.2008.05.001

Viccaro, M., Ferlito, C., Cortesogno, L., Cristofolini, R., & Gaggero, L. (2006). Magma mixing during the 2001 event at Mt. Etna (Italy): Effects on the eruptive dynamics. *Journal of Volcanology and Geothermal Research*, *149*, 139–159. https://doi.org/10.1016/j.jvolgeores.2005.06.004

Viccaro, M., Giuffrida, M., Zuccarello, F., Scandura, M., Palano, M., & Gresta, S. (2019). Violent paroxysmal activity drives self-feeding magma replenishment at Mt. Etna. *Scientific Reports*, *9*, 6717. https://doi.org/10.1038/s41598-019-43211-9

Viccaro, M., & Zuccarello, F. (2017). Mantle ingredients for making the fingerprint of Etna alkaline magmas: Implications for shallow partial melting within the complex geodynamic framework of Eastern Sicily. *Journal of Geodynamics*, *109*, 10–23. https://doi.org/10.1016/j.jog.2017.06.002

Viccaro, M., Zuccarello, F., Cannata, A., Palano, M., & Gresta, S. (2016). How a complex basaltic volcanic system works: Constraints from integrating seismic, geodetic, and petrological data at Mount Etna volcano during the July–August 2014 eruption. *Journal of Geophysical Research: Solid Earth*, *121*, 5659–5678. https://doi.org/10.1002/2016JB013164

Wallace, P. J., Kamenetsky, V. S., & Cervantes, P. (2015). Melt inclusion CO_2 contents, pressures of olivine crystallization, and the problem of shrinkage bubbles. *American Mineralogist*, *100*, 787–794. https://doi.org/10.2138/am-2015-5029

SUPPORTING INFORMATION

Additional supporting information may be found online in the Supporting Information section.

How to cite this article: Zuccarello F, Schiavi F, Viccaro M. Magma dehydration controls the energy of recent eruptions at Mt. Etna volcano. *Terra Nova*. 2021;33:423–429. https://doi.org/10.1111/ter.12527